ISSN 1063-7834, Physics of the Solid State, 2021, Vol. 63, No. 5, pp. 802–810. © Pleiades Publishing, Ltd., 2021.
ISSN 1063-7834, Physics of the Solid State, 2021. © Pleiades Publishing, Ltd., 2021.
Russian Text © The Author(s), 2021, published in Fizika Tverdogo Tela, 2021, Vol. 63, No. 6, pp. 754–762.

Synthesis and Structural and Magnetic Properties of the $NaNiFe_2(VO_4)_3$ Compound

T. V. Drokina[a, *], D. A. Velikanov[a], O. A. Bayukov[a], M. S. Molokeev[a, b], and G. A. Petrakovskii[a]

[a] *Kirensky Institute of Physics, Krasnoyarsk Scientific Center, Siberian Branch, Russian Academy of Sciences, Krasnoyarsk, 660036 Russia*

[b] *Siberian Federal University, Krasnoyarsk, 660041 Russia*

**e-mail: tvd@iph.krasn.ru*

Received February 8, 2021; revised February 8, 2021; accepted February 11, 2021

Abstract—A new magnetic compound $NaNiFe_2(VO_4)_3$ has been obtained by the solid-phase synthesis and studied by X-ray diffractometry, nuclear gamma resonance, and magnetometry. The crystal structure of multicomponent vanadate is described by a triclinic symmetry space group $P\bar{1}$. The unit cell contains six nonequivalent mixed cationic positions occupied by different-valence ions of transition metals, iron Fe^{3+} and nickel Ni^{2+}, which facilitates the implementation of a state with the local charge neutrality violation. In addition, two types of iron atom sites have been found, which have an oxygen environment in the form of octahedra and square pyramids with their nonequiprobable population by iron and nickel. The temperature and field dependences of the magnetization have been found to be typical of a paramagnet containing ferromagnetic clusters in a wide temperature range.

Keywords: multicomponent vanadates, crystal structure, magnetic properties

DOI: 10.1134/S1063783421060056

1. INTRODUCTION

Crystallochemical features of the vanadium-containing complex oxides offer wide opportunities for synthesis of new compounds with intriguing physical properties, which open prospects for new applications. The interest in studying multicomponent vanadates is largely due to the peculiarity of their crystal structure, which allows the existence of competing magnetic interactions and the formation of different types of magnetic ordering [1–5]. In this context, it is interesting to search for new compounds based on vanadium and transition metals.

The structural properties of the compounds with the general chemical formula $ACuFe_2(VO_4)_3$ (A is the monovalent alkaline earth element (Na or Li)) were studied in [2, 4, 6, 7]. The results of the studies showed that, at room temperature, the $LiCuFe_2(VO_4)_3$ and $NaCuFe_2(VO_4)_3$ crystal structures are described by the triclinic symmetry space group $P\bar{1}$ and the unit cell contains two nonequivalent octahedral iron sites Fe1 and Fe2. It was demonstrated that the substitution of sodium for lithium in the $ACuFe_2(VO_4)_3$ (A = Na, Li) system leads to the transformation of the crystal lattice parameters, distances between magnetic ions, and crystallite size [2].

The magnetism of the $LiCuFe_2(VO_4)_3$ compound is characterized mainly by the antiferromagnetic exchange interaction and the high level of frustrations in a chain spin structure [4]. In the framework of the indirect coupling model, the parameters of exchange interactions effects were estimated in the six-sublattice representation of the $LiCuFe_2(VO_4)_3$ magnet. It was shown that the compound is an antiferromagnet with the strong intrachain and frustrating interchain exchange couplings [4].

An interesting feature in the properties of the $LiCuFe_2(VO_4)_3$ compound, in contrast to $NaCuFe_2(VO_4)_3$, is the magnetodielectric effect: an external magnetic field leads to an increase in the permittivity [8, 9].

The data of the static magnetic investigations of howardevansite $NaCuFe_2(VO_4)_3$ showed that, in this compound, the disordered magnetic state is implemented at low temperatures, along with paramagnetism and antiferromagnetism [2, 8]. The estimation of the exchange interaction parameters revealed the strong intrachain and weak interchain exchange couplings [8].

The resonance properties of the $LiCuFe_2(VO_4)_3$ and $NaCuFe_2(VO_4)_3$ compounds were examined in the temperature range of 110–300 K in the *X* band; the electron spin resonance with a *g* factor of 2 was detected [2, 4].

The experiments showed that the competition of the exchange interactions of different signs and values and the nonuniform distribution of iron cations over nonequivalent crystallographic sites lead to the dependence of the magnetic properties of the $ACuFe_2(VO_4)_3$ (A = Na, Li) system on its composition.

It can be expected that the incorporation of different transition metal ions into the structure of complex vanadates will change their crystal lattice and ways of overlapping the *d* orbitals of transition elements with the orbitals of neighboring atoms, affecting the magnetic properties. The aim of this study is to obtain a new oxide material with the $NaNiFe_2(VO_4)_3$ composition and experimentally investigate its properties. We report on the measured structural and magnetic characteristics of the complex vanadate containing ions of transition elements.

2. EXPERIMENTAL

The new $NaNiFe_2(VO_4)_3$ compound was obtained by the solid-state reaction from a mixture of the high-purity Na_2CO_3, Fe_2O_3, NiO, and V_2O_5 oxides taken in a stoichiometric ratio:

$$1/2(Na_2CO_3) + Fe_2O_3 + NiO + 3/2(V_2O_5) \rightarrow NaNiFe_2(VO_4)_3.$$

Samples in the form of tablets with a diameter of 10 mm and a thickness of 1.5–2.0 mm pressed from a reagent mixture were treated at temperatures of 600–640°C in air. The chemical and phase compositions of the synthesized compound was controlled by X-ray diffractometry.

An X-ray powder diffraction pattern of $NaNiFe_2(VO_4)_3$ was obtained at room temperature on a Bruker D8 ADVANCE diffractometer using a VANTEC linear detector (CuK_α radiation). The Rietveld refinement was performed using the TOPAS 4.2 program [10]. In the X-ray diffraction experiment, different primary beam slit sizes were used: 0.6 mm in the angular range of $2\theta = 5°–70°$ and 2 mm in the range of 70°–120°. A scanning step of 0.016° was the same in all the regions; the exposure time at each step was 3 s. After that, the standard deviations of the intensities of all points of the X-ray diffraction pattern were calculated and, then, the intensities and standard deviations of all points of the high-angle part were multiplied by a normalization factor of 0.6.

Mössbauer spectra were detected on an MS-1104Em spectrometer at the Research Institute of Physics of the Southern Federal University in the transmission geometry with a Co^{57}(Rh) radioactive source at room temperature on a powder sample with a composition of 5–10 mg/cm^2 from the natural iron content.

The static magnetic characteristics of the samples were measured on original magnetometers at the Kirensky Institute of Physics, Krasnoyarsk Scientific Center, Siberian Branch of the Russian Academy of Sciences [11, 12]: on a SQUID magnetometer in the temperature range of 4–300 K in a magnetic field of $H = 0–2$ kOe and on an automated vibrating sample magnetometer in the temperature range of 77–830 K in magnetic fields of up to 25 kOe. The temperature dependence of the magnetic moment was measured in magnetic fields of $H = 0$, 1000, 2000, and 2200 Oe. The hysteresis loops were obtained at temperatures of $T = 830$ and 77 K and at room temperature.

3. RESULTS AND DISCUSSION

3.1. Structural Properties of the $NaNiFe_2(VO_4)_3$ Compound

Figure 1 shows the X-ray powder diffraction pattern of the synthesized $NaNiFe_2(VO_4)_3$ compound obtained at room temperature.

Almost all reflections in the X-ray diffraction pattern of the sample were identified in a triclinic cell with lattice parameters of $a = 6.7559(1)$ Å, $b = 8.1309(2)$ Å, $c = 9.8098(2)$ Å, $\alpha = 106.346(2)°$, $\beta = 104.300(2)°$, $\gamma = 102.143(2)°$, and $V = 477.83(2)$ Å^3, which are similar to those of $NaFe_3(VO_4)_3$, i.e., $a = 6.757(2)$ Å, $b = 8.155(2)$ Å, $c = 9.816(3)$ Å, $\alpha = 106.05(2)°$, $\beta = 104.401(9)°$, $\gamma = 102.09(2)°$, and $V = 480.46$ Å^3 [13]; therefore, the $NaFe_3(VO_4)_3$ structure was used as initial. Since the refinement of the population of Fe/Ni sites was very unstable because of the closeness of atomic scattering functions, all the six sites of Fe cations were populated by Fe/Ni cations with fixed site populations, according to the chemical formula Fe/Ni = 2 : 1. Coordinates of Na1 were not refined, which is necessary to fix the origin of coordinates in the polar group *P*1. The main crystallographic

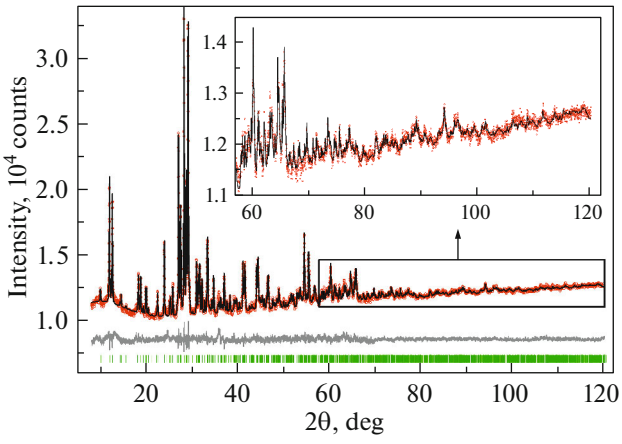

Fig. 1. X-ray diffraction pattern of the polycrystalline $NaNiFe_2(VO_4)_3$ compound at room temperature. The difference X-ray diffraction pattern is the lower curve.

Table 1. Main parameters of the X-ray experiment conducted at a temperature of $T = 300$ K and results of refinement of the $NaNiFe_2(VO_4)_3$ crystal structure

Sp. gr.	P_1
a, Å	6.7559 (1)
b, Å	8.1309 (2)
c, Å	9.8098 (2)
α, deg	106.346 (2)
β, deg	104.300 (2)
γ, deg	102.143 (2)
V, Å^3	477.83 (2)
2θ range, deg	5–120
Number of reflections	1473
Number of refined parameters	160
R_{wp}, %	0.97
R_p, %	0.87
R_B, %	0.42
χ^2	1.50

a, b, c, α, β, and γ are the unit cell parameters; V is the cell volume; R_{wp}, R_p, and R_B are the weight, profile, and integral infidelity factors, respectively; and χ^2 is the fitting quality.

characteristics of $NaNiFe_2(VO_4)_3$ and parameters of the X-ray experiment are given in Table 1.

The crystal structure of the $NaNiFe_2(VO_4)_3$ oxygen compound is described by the triclinic space group $P1$, different from $P\bar{1}$, which characterizes the vanadates $LiCuFe_2(VO_4)_3$ and $NaCuFe_2(VO_4)_3$. The unit cell of the investigated compound contains two formula units

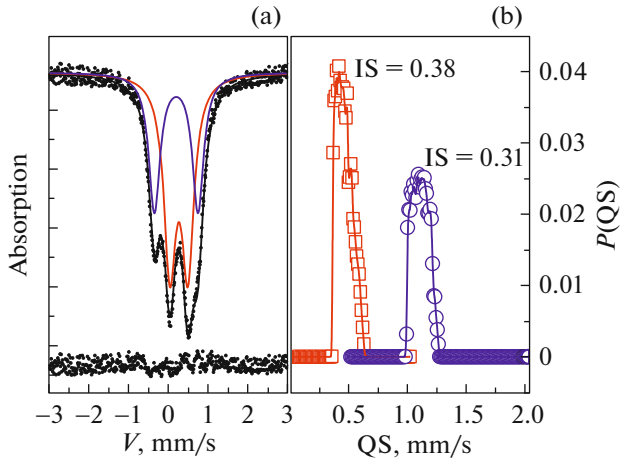

Fig. 2. (a) Mössbauer spectrum of the $NaNiFe_2V_3O_{12}$ compound measured at room temperature. Colored lines show the spectral components the parameters of which are given in Table 4. (b) Quadrupole splitting probability distribution in the experimental spectrum.

($Z = 2$). The independent part of the $NaNiFe_2(VO_4)_3$ cell ($P1$) coincides with the elementary one, in contrast to the structures in the $P\bar{1}$ group, where the independent part of the cell is twice as small and the number of independent atoms is also twice as small. It is the presence/absence of the inversion center that leads to such differences. In all the other respects, the structures are not fundamentally different.

The atomic coordinates, occupancies of sites in the $NaNiFe_2(VO_4)_3$ crystal structure, and thermal parameters of the experiment are given in Table 2 and the main bond lengths in the crystal lattice are given in Table 3. The charge composition of the compound is $Na^+Ni^{2+}Fe_2^{3+}(V^{5+}O_4)_3$.

According to the X-ray diffraction study, iron cations Fe^{3+} in the unit crystal cell of $NaNiFe_2(VO_4)_3$ occupy six crystallographically nonequivalent sites populated together with nickel cations Ni^{2+} (Table 2). Four of these six Fe/Ni sites have oxygen coordination 6 (octahedron) and two sites, coordination 5 (trigonal bipyramid). Thus, a feature of the crystal structure of the investigated compound is the localization of cations of different types and valences in the same crystal site. This leads to the fact that, depending on the ratio between iron and nickel ions in one crystallographic site, an excess or a lack of a positive charge forms, i.e., the state of local charge neutrality violation is implemented.

To obtain additional information on the structure and characterize the state of iron in the substance, the $NaNiFe_2(VO_4)_3$ sample was studied using the Mössbauer effect. Figure 2a shows the room-temperature Mössbauer spectrum of the $NaNiFe_2(VO_4)_3$ polycrystal. The spectrum was processed in two stages. At the first stage, the distribution of the quadrupole splitting probability P(QS) in the experimental spectrum was determined (Fig. 2b). At the second stage, basing on the data obtained from the P(QS) distribution, a model spectrum was built and fitted to the experimental spectrum by varying all hyperfine parameters by the least squares method in the linear approximation. The fitting result is given in Table 4.

The distribution of the quadrupole splitting probability in the spectrum (Fig. 2b) indicates the presence of two types of iron atom sites with different chemical shifts and quadrupole splittings. According to the X-ray diffraction data, the sites with parameters of IS = 0.38 mm/s and QS = 0.45 mm/s should be attributed to the octahedral oxygen environments of cations $Fe^{3+}(6)$ in $NaNiFe_2V_3O_{12}$. The sites of iron ions in the oxygen environment in the form of trigonal pyramids have a smaller coordination number and, therefore, a smaller chemical shift, as well as a significant degree of distortion of the local environment, i.e., a larger quadrupole splitting. These conditions are met by the sites with Mössbauer parameters of IS = 0.31 mm/s and QS = 1.10 mm/s (Table 4). Thus,

Table 2. Atomic coordinates, isotropic thermal parameters B_{iso} (Å^2), and site occupancy Occ. in the crystal structure of the $NaNiFe_2(VO_4)_3$ compound at a temperature of $T = 300$ K

Atom	*x/a*	*y/b*	*z/c*	B_{iso}	Occ.
Na1	0.99425	0.07762	0.5534	3 (1)	1
Na2	0.462 (9)	1.018 (7)	0.492 (7)	0.5 (7)	1
Fe1	0.111 (7)	0.551 (5)	0.400 (5)	0.3 (2)	0.667
Ni1	0.111 (7)	0.551 (5)	0.400 (5)	0.3 (2)	0.333
Fe2	0.879 (7)	0.448 (5)	0.610 (5)	0.3 (2)	0.667
Ni2	0.879 (7)	0.448 (5)	0.610 (5)	0.3 (2)	0.333
Fe3	0.458 (7)	0.318 (5)	0.984 (5)	0.3 (2)	0.667
Ni3	0.458 (7)	0.318 (5)	0.984 (5)	0.3 (2)	0.333
Fe4	0.546 (7)	0.733 (4)	0.021 (5)	0.3 (2)	0.667
Ni4	0.546 (7)	0.733 (4)	0.021 (5)	0.3 (2)	0.333
Fe5	0.796 (7)	0.767 (4)	0.784 (5)	0.3 (2)	0.667
Ni5	0.796 (7)	0.767 (4)	0.784 (5)	0.3 (2)	0.333
Fe6	0.234 (7)	0.222 (5)	0.192 (5)	0.3 (2)	0.667
Ni6	0.234 (7)	0.222 (5)	0.192 (5)	0.3 (2)	0.333
V1	0.392 (8)	0.419 (5)	0.664 (6)	0.5 (2)	1
V2	0.606 (8)	0.594 (5)	0.329 (5)	0.5 (2)	1
V3	0.280 (7)	0.839 (5)	0.732 (5)	0.5 (2)	1
V4	0.730 (7)	0.168 (5)	0.261 (5)	0.5 (2)	1
V5	0.090 (7)	0.777 (5)	0.131 (5)	0.5 (2)	1
V6	0.902 (7)	0.216 (5)	0.879 (5)	0.5 (2)	1
O1	0.427 (17)	0.442 (11)	0.864 (11)	0.5 (2)	1
O2	0.577 (17)	0.555 (11)	0.139 (11)	0.5 (2)	1
O3	0.366 (17)	0.487 (11)	0.344 (11)	0.5 (2)	1
O4	0.629 (16)	0.537 (11)	0.649 (11)	0.5 (2)	1
O5	0.268 (13)	0.80 (1)	0.56 (1)	0.5 (2)	1
O6	0.743 (14)	0.195 (11)	0.46 (1)	0.5 (2)	1
O7	0.500 (17)	0.22 (1)	0.16 (1)	0.5 (2)	1
O8	0.498 (16)	0.76 (1)	0.828 (11)	0.5 (2)	1
O9	0.149 (16)	0.26 (1)	0.009 (11)	0.5 (2)	1
O10	0.843 (16)	0.73 (1)	0.994 (11)	0.5 (2)	1
O11	0.180 (14)	0.46 (1)	0.58 (1)	0.5 (2)	1
O12	0.838 (14)	0.51 (1)	0.41 (1)	0.5 (2)	1
O13	0.019 (17)	0.721 (12)	0.739 (12)	0.5 (2)	1
O14	0.977 (17)	0.286 (11)	0.261 (11)	0.5 (2)	1
O15	0.319 (17)	0.054 (12)	0.824 (11)	0.5 (2)	1
O16	0.682 (17)	0.959 (12)	0.177 (11)	0.5 (2)	1
O17	0.343 (15)	0.193 (11)	0.58 (1)	0.5 (2)	1
O18	0.666 (17)	0.791 (11)	0.42 (1)	0.5 (2)	1
O19	0.187 (17)	0.012 (11)	0.24 (1)	0.5 (2)	1
O20	0.82 (2)	0.999 (11)	0.78 (1)	0.5 (2)	1
O21	0.282 (15)	0.734 (11)	0.04 (1)	0.5 (2)	1
O22	0.734 (15)	0.270 (11)	0.969 (11)	0.5 (2)	1
O23	0.066 (15)	0.655 (11)	0.232 (8)	0.5 (2)	1
O24	0.926 (15)	0.332 (11)	0.746 (9)	0.5 (2)	1

Table 3. Main bond lengths (Å) in the $NaNiFe_2(VO_4)_3$ crystal structure: (i) $x+1, y, z$; (ii) $x, y+1, z$; (iii) $x-1, y, z$; (iv) $x, y, z+1$; (v) $x, y, z-1$; (vi) $x, y-1, z$; (vii) $x-1, y, z-1$; and (viii) $x+1, y, z+1$

Na1–O6	2.26 (6)	Ni4–O8^{v}	1.9 (1)
Na1–O17^{i}	2.27 (6)	Ni4–O10^{v}	2.09 (7)
Na2–O6^{ii}	2.29 (6)	Ni4–O16	1.89 (9)
Na2–O17^{ii}	1.88 (7)	Ni4–O21	1.85 (7)
Fe1–O3	2.05 (8)	Fe5–O4	1.87 (8)
Fe1–O5	2.07 (8)	Fe5–O8	2.15 (7)
Fe1–O11	2.04 (8)	Fe5–O10	2.1 (1)
Fe1–O12^{iii}	1.85 (6)	Fe5–O13^{i}	1.76 (7)
Fe1–O14^{iii}	2.06 (8)	Fe5–O20	1.89 (6)
Fe1–O23	2.04 (8)	Ni5–O4	1.87 (8)
Ni1–O3	2.05 (8)	Ni5–O8	2.15 (7)
Ni1–O5	2.07 (8)	Ni5–O10	2.1 (1)
Ni1–O11	2.04 (8)	Ni5–O13^{i}	1.76 (7)
Ni1–O12^{iii}	1.85 (6)	Ni5–O20	1.89 (6)
Ni1–O14^{iii}	2.06 (8)	Fe6–O3	2.10 (8)
Ni1–O23	2.04 (8)	Fe6–O7	1.88 (8)
Fe2–O4	2.05 (7)	Fe6–O9	1.88 (10)
Fe2–O6	2.03 (8)	Fe6–O14^{iii}	2.13 (8)
Fe2–O11^{i}	2.13 (6)	Fe6–O19	1.87 (6)
Fe2–O12	2.10 (9)	Ni6–O3	2.10 (8)
Fe2–O13^{i}	2.09 (8)	Ni6–O7	1.88 (8)
Fe2–O24	1.85 (8)	Ni6–O9	1.88 (10)
Ni2–O4	2.05 (7)	Ni6–O14^{iii}	2.13 (8)
Ni2–O6	2.03 (8)	Ni6–O19	1.87 (6)
Ni2–O11^{i}	2.13 (6)	V1–O1	1.87 (11)
Ni2–O12	2.10 (9)	V1–O4	1.75 (7)
Ni2–O13^{i}	2.09 (8)	V1–O11	1.64 (7)
Ni2–O24	1.85 (8)	V1–O17	1.71 (7)
Fe3–O1	1.76 (8)	V2–O2	1.75 (11)
Fe3–O2^{iv}	1.94 (9)	V2–O3	1.73 (7)
Fe3–O7^{iv}	2.09 (8)	V2–O12	1.92 (7)
Fe3–O9^{iv}	2.13 (7)	V2–O18	1.50 (7)
Fe3–O15	2.12 (9)	V3–O5	1.56 (9)
Fe3–O22	2.01 (6)	V3–O8	1.87 (7)
Ni3–O1	1.76 (8)	V3–O13	1.85 (7)
Ni3–O2^{iv}	1.94 (9)	V3–O15^{ii}	1.66 (8)
Ni3–O7^{iv}	2.09 (8)	V4–O6	1.8 (1)
Ni3–O9^{iv}	2.13 (7)	V4–O7	1.83 (8)
Ni3–O15	2.12 (9)	V4–O14	1.74 (7)
Ni3–O22	2.01 (6)	V4–O16^{vi}	1.59 (8)
Fe4–O1^{v}	2.27 (8)	V5–O10^{vii}	1.75 (9)
Fe4–O2	2.11 (7)	V5–O19^{ii}	1.79 (7)
Fe4–O8^{v}	1.9 (1)	V5–O21	1.77 (7)
Fe4–O10^{v}	2.09 (7)	V5–O23	1.60 (7)
Fe4–O16	1.89 (9)	V6–O9^{viii}	1.73 (9)
Fe4–O21	1.85 (7)	V6–O20^{vi}	1.66 (7)
Ni4–O1^{v}	2.27 (8)	V6–O22	1.66 (8)
Ni4–O2	2.11 (7)	V6–O24	1.83 (8)

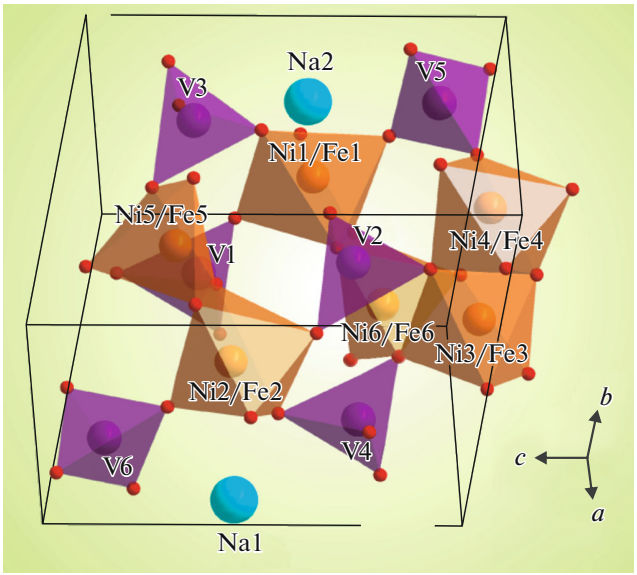

Fig. 3. $NaNiFe_2(VO_4)_3$ crystal structure.

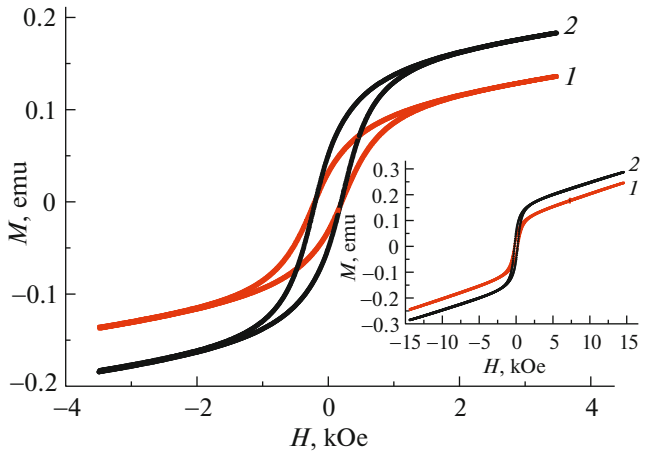

Fig. 4. Magnetic hysteresis loops in $NaNiFe_2V_3O_{12}$ at room temperature. Samples with masses of m = (*1*) 0.160 g and (*2*) 0.140 g. Inset: behavior of the magnetic moment in magnetic fields of up to 20 kOe.

~60% of iron atoms included in $NaNiFe_2V_3O_{12}$ are located in the octahedra and ~40%, in the trigonal pyramids. The occupancies of sites with iron were estimated under the assumption of the equal probability of the Mössbauer effect for the octahedral and prismatic sites. The absence of a Gaussian form of the P(QS), distributions in Fig. 2b can evidence for the nonequiprobable population of the octahedral and prismatic sites by iron and nickel, respectively.

Thus, the nuclear gamma resonance refinement of the structural features of $NaNiFe_2(VO_4)_3$ showed that iron cations Fe^{3+} are in the high-spin state S = 5/2 and occupy the sites of two types with different oxygen environments: octahedral and in the form of trigonal bipyramids. Hence, ~80% of nickel is located in the octahedra and ~20%, in trigonal pyramids, so the vanadate formula can be presented in the form

$$Na[Fe_{1.2}Ni_{0.8}]\{Fe_{0.8}Ni_{0.2}\}(VO_4)_3,$$

where the square brackets contain the octahedral sites and the curly brackets, the pyramidal sites.

Thus, based on the X-ray diffraction and Mössbauer data, it can be assumed that, in the crystal structure of the $NaNiFe_2(VO_4)_3$ compound, octahedra $(Fe1/Ni1)O_6$, $(Fe2/Ni2)O_6$, $(Fe3/Ni3)O_6$, and $(Fe4/Ni4)O_6$ and trigonal bipyramids $(Fe5/Ni5)O_5$ and $(Fe6/Ni6)O_5$ are edge-sharing and form endless chains (...–(Fe1/Ni1)–(Fe2/Ni2)–(Fe5/Ni5)–(Fe4/Ni4)–(Fe3/Ni3)–(Fe6/Ni6)–...) stretched in the **a**–**c** direction. In addition, the octahedra and trigonal bipyramids share vortices with vanadium tetrahedra VO_4. The infinite chains ...–Fe/Ni–Fe/Ni–... are sewed together with VO_4 tetrahedra into a two-dimensional layer located in the plane defined by two vectors: **a**–**c** and **b**. These layers, in turn, are joint by VO_4 with the formation of a three-dimensional structure (frame). The crystal structure of vanadate $NaNiFe_2(VO_4)_3$ is shown in Fig. 3.

Table 4. Mössbauer parameters of $NaNiFe_2V_3O_{12}$. IS is the isomer shift relative to α-Fe, QS is the quadrupole splitting, W is the absorption linewidth, and A is the area under the partial spectrum (fractional occupancy of the nonequivalent site with iron)

IS, mm/s ±0.02	QS, mm/s ±0.04	W, mm/s ±0.04	A, at % ±0.03	Site
0.38	0.45	0.37	0.59	Fe^{3+} (6)
0.31	1.10	0.34	0.41	Fe^{3+} (5)

3.2. Magnetic Characteristics of $NaNiFe_2(VO_4)_3$

Magnetism in the multicomponent $NaNiFe_2V_3O_{12}$ system is governed by iron ions Fe^{3+} (electron configuration $3d^5$ and spin S = 5/2) and nickel ions Ni^{2+} ($3d^8$, S = 3/2). In this compound, vanadium is pentavalent, V^{5+} (d^0) and there is no magnetic moment.

Figures 4–8 show the experimental data characterizing the magnetic properties of $NaNiFe_2V_3O_{12}$.

The results of the study showed that the field dependence of the magnetic moment $M(H)$ for $NaNiFe_2V_3O_{12}$ at room temperature is nonlinear and hysteretic (Fig. 4). The opening of the magnetic hysteresis loop is observed in magnetic fields of $|H| <$ 2 kOe. Thus, the characteristics of the magnetic behavior of the $NaNiFe_2V_3O_{12}$ samples are indicative of the ferromagnetic properties.

However, the presented data show also that the field dependence of the magnetic moment $M(H)$

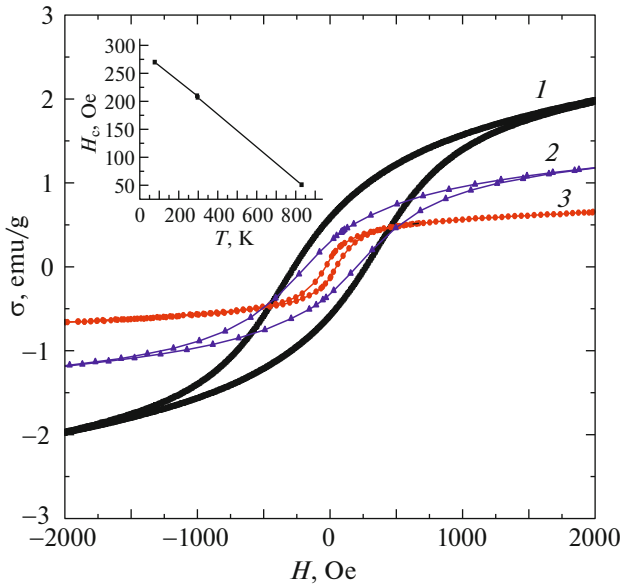

Fig. 5. Magnetic-field dependence of the static magnetization of $NaNiFe_2(VO_4)_3$ measured at temperatures of T = 77 K (curve *1*), 300 K (curve *2*), and 830 K (curve *3*). Inset: temperature dependence of coercivity H_c.

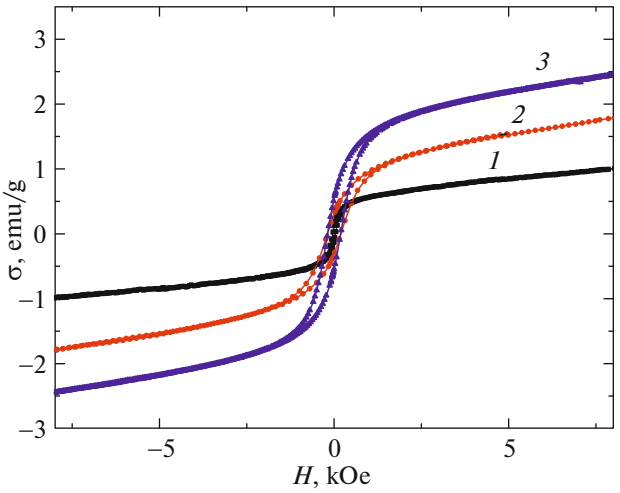

Fig. 6. Dependence of the magnetic characteristics of the $NaNiFe_2V_3O_{12}$ sample on its thermomagnetic prehistory at temperatures of 830 K (curve *1*) and 300 K (curve *2* measured before heating the sample and curve *3*, after heating the sample to 830 K).

reveals a significant increase in the magnetic moment in magnetic fields above the technical saturation (the paraprocess region) (Fig. 4). As is known [14], in many ferromagnets the magnetization in the paraprocess region increases insignificantly and its growth is caused by a change in the orientation of the spin moments of individual electrons located inside the spontaneous magnetization regions (domains) and the regions that did not rotate in the field direction due to the effect of thermal motion. In the investigated material with a crystal structure containing six different mixed sites of magnetic cations, the magnetization processes, including the displacement of domain walls, rotation of the magnetic moments of domains in the applied magnetic field direction, and the paraprocess, can be expected to partially overlap, leading to an increase in the magnetic moment in the above-saturation fields. However, the magnetization increment in magnetic fields above 2 kOe is large and follows, most likely, from the manifestation of the paramagnetic properties of the material under study.

Figure 5 shows the measured field dependences of the magnetization of $NaNiFe_2V_3O_{12}$ at temperatures of 77, 300, and 830 K. The coercivity H_C at room temperature is ~200 Oe; at the transition to a temperature of T = 830 K, its value decreases by a factor of 4. In addition, the experimental data show that the temperature lowering down to 77 K leads to an increase in the magnetic field required to demagnetize the $NaNiFe_2V_3O_{12}$ material. Probably, the sample imperfection, which affects the dynamics of motion of domains and domain walls is the main factor that determines the magnetic hysteresis in $NaNiFe_2V_3O_{12}$. Note that, under magnetization reversal in the opposite direction, the H_c value differs by about 10–20 Oe. The latter feature is apparently related to the thermomagnetic prehistory of the sample. The inset in Fig. 5 shows the temperature dependence of the coercivity H_C in $NaNiFe_2V_3O_{12}$.

Thus, according to the magnetic measurement data, on the one hand, the H_c value increases with decreasing temperature, which is typical of most ferromagnetic materials. On the other hand, the field dependences of the static magnetization of $NaNiFe_2(VO_4)_3$ measured at different temperatures reveal the slope change in magnetic fields above 2 kOe upon temperature variation (Fig. 5), which is characteristic of a paramagnetic material.

The analysis of the magnetization curves of $NaNiFe_2V_3O_{12}$ at temperatures of T = 300 and 830 K (curve *3* in Fig. 6) shows the dependence of the magnetization value on the experimental conditions. At room temperature, the field dependence of the magnetization was measured twice: before heating the sample to a temperature of T = 830 K (curve *2*) and after it (curve *1*). Cooling the sample to room temperature after heating to 830 K leads to an increase in the magnetization by ~40% in a magnetic field of 2 kOe. The change in the magnetization caused by the heat treatment of the sample is retained in stronger magnetic fields (H = 10 kOe). In this case, the coercivity remains unchanged.

Thus, according to the experimental data, the sample under study exhibits both the ferro- and paramagnetic properties. It is interesting to conduct the experiment that would exclude the impact of the paramag-

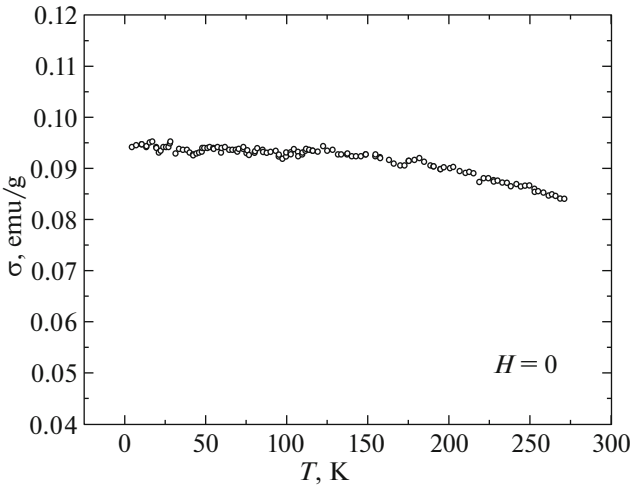

Fig. 7. Temperature dependence of the remanent magnetization of $NaNiFe_2(VO_4)_3$. The sample mass is $m = 0.120$ g.

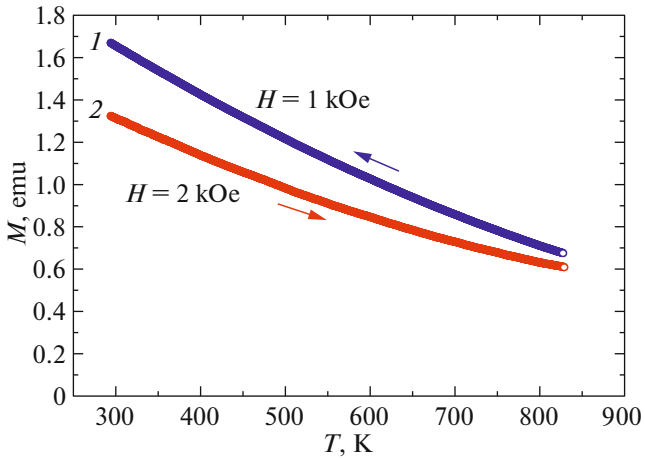

Fig. 8. Temperature dependences of the magnetic moment of $NaNiFe_2(VO_4)_3$ measured in magnetic fields of $H = 1$ and 2 kOe in the temperature range of 300–830 K in the sample cooling (curve *1*) and heating (curve *2*) modes.

netic component of the magnetization on the magnetic characteristics of the sample. To do that, we measured the temperature dependence of the remanent magnetization in the temperature range from helium to room. Figure 7 presents the temperature dependence of the remanent magnetization of $NaNiFe_2V_3O_{12}$ measured on a SQUID magnetometer without external magnetic field H. According to the measurement data, the shape of the curve in Fig. 7 is typical of a magnet with the ferromagnetic ordering and the spontaneous magnetization of the sample is $\sigma_{T=0} = 0.095$ emu/g ($T = 0$ K).

Note also the features in the behavior of the $NaNiFe_2V_3O_{12}$ compound that are related to its thermomagnetic prehistory. Figure 8 shows temperature dependences of the magnetic moment measured in magnetic fields of $H = 1000$ and 2000 Oe in the temperature range of 300–830 K upon cooling and heating the $NaNiFe_2V_3O_{12}$ sample. The experimental data show that the magnetic moment of the sample at room temperature increases by ~27% after heating from 300 to 830 K, despite the difference in the applied magnetic fields.

The interpretation of the properties of vanadate $NaNiFe_2(VO_4)_3$ with a complex composition and crystallographic structure faces certain difficulties caused by the presence of six nonequivalent crystallographic sites Fe*i*/Ni*i* ($i = 1$–6) and localization of different valence cations in them, which are nonuniformly populated and lead to the structural inhomogeneity. In addition, upon embedding of nickel ions into the sites of iron ions, the difference in their ionic radii r ($r_{Fe^{3+}} = 0.67$ Å and $r_{Ni^{2+}} = 0.78$ Å) causes crystal lattice distortions.

It should be noted that the solid-state synthesis of samples from mixtures of powdered oxides can lead to the formation of secondary products, including magnetic ones. The difficulties of the interpretation of the experimental data related to the presence of impurities require their possible impact on the $NaNiFe_2(VO_4)_3$ magnetic properties to be analyzed. A probable impurity is hematite α-Fe_2O_3. As is known [15–17], hematite is a rhombohedral antiferromagnet with a Néel temperature of $T_N = 950$ K; in the vicinity of $T_M \approx 260$ K (the Morin temperature), the spin reorientation with a rotation by 90° occurs and the noncollinear spin ordering with a cant of 5° relative to each other is established, which evokes weak magnetism. Analyzing the possible effect of the α-Fe_2O_3 impurity on the magnetic properties of the investigated $NaNiFe_2(VO_4)_3$ samples, note that no anomalies of the magnetic properties were found in the vicinity of $T_M \approx 260$ K, which corresponds to the Morin spin-reorientation transition between the collinear antiferromagnetic and weakly ferromagnetic states. Among possible impurities that were not detected in the course of our experiments is magnetite Fe_3O_4, a compound with an inverse spinel structure $Fe^{3+}[Fe^{2+}Fe^{3}]O_4$. At room temperature, ferrite Fe_3O_4 is a ferrimagnet; the ferrimagnetic ordering is destructed by thermal motion at temperatures of 850–860 K; the coercivity is $H_c = 2.1$ Oe [18, 19]. At a temperature of $T = 100$–120 K (the Verwey temperature), magnetite undergoes a low-temperature structural transformation, which is reflected in the temperature dependences of the magnetization, heat capacity, and resistivity [18, 19]. In the $NaNiFe_2(VO_4)_3$ sample, no anomaly was found in the temperature dependence of the magnetic moment $M(T)$ at $T = 100$–120 K. In addition, note that, according to the Mössbauer data, there are no Fe^{2+} cations in the samples under study. The solid-state

reaction by-products that can be considered are nickel ferrite $NiFe_2O_4$ and nickel oxide NiO, The $NiFe_2O_4$ compound has an inverted spinel crystal structure, a Curie temperature of $T_C = 863$ K, and the coercivity of $H_c = 5$ Oe. The NiO cubic crystal is an antiferromagnet with a Néel temperature of $T_N = 793$ K [18]. Thus, the analysis of the properties of probable impurities shows that the characteristics of the magnetism of the synthesized $NaNiFe_2(VO_4)_3$ compound differ from those of the possible solid-state reaction by-products.

In addition, we measured the specific heat by an adiabatic calorimeter method in the mode of continuous heating in the temperature range of 77–870 K. In this temperature range, there are no features in the temperature dependence of specific heat that would be indicative of phase transformations in the sample.

Thus, the main features of the synthesized $NaNiFe_2V_3O_{12}$ sample, which characterizes its magnetic properties, is the presence of a magnetic moment dependent on temperature (Figs. 5 and 7), magnetic field (Figs. 4, 5), and thermomagnetic prehistory (Figs. 6, 8). The analysis of the magnetic characteristics of $NaNiFe_2(VO_4)_3$ shows that the material, along with the ferromagnetic properties, exhibits the properties of a paramagnet. The set of experimental facts can be explained under the assumption that the sample is a paramagnetic matrix with ferromagnetic inclusions (clusters). The latter determine the ferromagnetic behavior of the sample. In this concept, an increase in the magnetization after "annealing" in a magnetic field apparently indicates not only the alignment of individual magnetic particles of the material along the applied magnetic field direction and an increase in their volume, but also the formation of new ferromagnetic inclusions. In addition, note that a decrease in the remanent magnetization with increasing temperature is observed. However, the Curie temperature of the ferromagnetic formations is apparently much higher than the maximum temperature (830 K) obtained in the experiment. It can be assumed that the interaction between iron and nickel ions occupying different $NaNiFe_2(VO_4)_3$ crystal lattice sites leads to the formation of an inhomogeneous system of ferromagnetic clusters, the properties of which may depend, in particular, on the iron–iron, nickel–nickel, and iron–nickel interionic spacings. The ordering of clusters, the nature of which is unclear and requires additional research, significantly affects the formation of the magnetic properties of the material under study in a wide temperature range.

4. CONCLUSIONS

The new vanadium oxide $NaNiFe_2(VO_4)_3$ was obtained by the solid-state synthesis and studied by X-ray diffractometry, nuclear gamma resonance, and magnetometry. Basing on the above, the following conclusions can be drawn.

It was found that the samples have a triclinic crystal structure with sp. gr. $P1$ and lattice parameters of $a = 6.7559(1)$ Å, $b = 8.1309(2)$ Å, $c = 9.8098(2)$ Å, $\alpha = 106.346(2)°$, $\beta = 104.300(2)°$, $\gamma = 102.143(2)°$, and $V = 477.83(2)$ Å^3. The $NaNiFe_2(VO_4)_3$ structure has six nonequivalent mixed sites with the localization of cations of different types and valences (Fe^{3+}/Ni^{2+}) in the same site.

Iron ions in $NaNiFe_2V_3O_{12}$ are in the high-spin trivalent state and occupy octahedral (~60%) and pyramidal (~40%) sites nonequiprobably populated by iron and nickel atoms. Thus, the formula of the compound is $Na[Fe_{1.2}Ni_{0.8}]\{Fe_{0.8}Ni_{0.2}\}(VO_4)$, where square brackets contain octahedral sites and curly brackets, pyramidal sites.

The analysis of the magnetic properties of $NaNiFe_2(VO_4)_3$ shows that both the temperature and field dependences of the magnetization demonstrate a superposition of the para- and ferromagnetic behavior. The physical nature of the features observed in the magnetism of $NaNiFe_2(VO_4)_3$ is possibly related to the magnetic interaction between iron and nickel ions with different and nonequiprobably populated crystal lattice sites, which facilitates the formation of magnetic clusters, the ordering of which leads to ferromagnetism.

ACKNOWLEDGMENTS

We are grateful to V.S. Bondarev for studying the thermal properties of $NaNiFe_2(VO_4)_3$.

CONFLICT OF INTEREST

The authors declare that they have no conflicts of interest.

REFERENCES

1. M. A. Lafontaine, J. M. Grenéche, Y. Laligant, and G. Férey, J. Solid State Chem. **108**, 1 (1994).
2. T. V. Drokina, G. A. Petrakovskii, O. A. Bayukov, M. S. Molokeev, A. M. Vorotynov, S. I. Popkov, and D. A. Velikanov, Phys. Solid State **62**, 297 (2020).
3. N. Guskos, G. Zolnierkiewicz, J. Typek, R. Szymczak, A. Guskos, P. Berczynski, and A. Blonska-Tabero, Mater. Sci. Poland **31**, 601 (2013).
4. T. V. Drokina, G. A. Petrakovskii, O. A. Bayukov, A. M. Vorotynov, D. A. Velikanov, and M. S. Molokeev, Phys. Solid State **58**, 1981 (2016).
5. G. Zolnierkiewicz, N. Guskos, J. Typek, E. A. Anagnostakis, A. Blonska-Tabero, and M. Bosacka, J. Alloys Compd. **471**, 28 (2009).
6. J. M. Hughes, J. W. Drexler, C. F. Campana, and M. L. Malinconico, Am. Mineral. **73**, 181 (1988).
7. A. A. Belik, Mater. Res. Bull. **34**, 1973 (1999).

8. A. V. Koshelev, K. V. Zakharov, L. V. Shvanskaya, A. A. Shakin, D. A. Chareev, S. Kamusella, H.-H. Klauss, K. Molla, B. Rahaman, T. Saha-Dasgupta, A. P. Pyatakov, O. S. Volkova, and A. N. Vasiliev, Phys. Rev. Appl. **10**, 034008 (2018).
9. T. V. Drokina, G. A. Petrakovskii, A. L. Freidman, M. S. Molokeev, and E. G. Rezina, RF Patent No. 2592867 (2016).
10. *Bruker AXS TOPAS V4: General Profile and Structure Analysis Software for Powder Diffraction Data, User's Manual* (Bruker AXS, Karlsruhe, Germany, 2008).
11. D. A. Velikanov, Vestn. SibGAU **2** (48), 176 (2013).
12. D. A. Velikanov, RF Patent No. 2341810 (2008).
13. F. D. Martin and H. Müller-Buschbaum, Z. Naturforsch. B **50**, 51 (1995).
14. K. P. Belov, *Elastic, Thermal and Electrical Phenomena in Ferromagnets* (Gos. Izdat. Tekh.-Teor. Liter., Moscow, 1957) [in Russian].
15. L. Néel and R. Pauthenet, C. R. Acad. Sci. Paris **234**, 2172 (1952).
16. L. Néel, Rev. Mod. Phys. **25**, 58 (1953).
17. J. O. Artman, J. C. Murphy, and S. Foner, Phys. Rev. A **138**, 912 (1965).
18. *Results of Science*, Vol. 4: *Antiferromagnetism and Ferrites* (Akad. Nauk SSSR, Moscow, 1962) [in Russian].
19. K. P. Belov, Phys. Usp. **36**, 53 (1993).

Translated by E. Bondareva